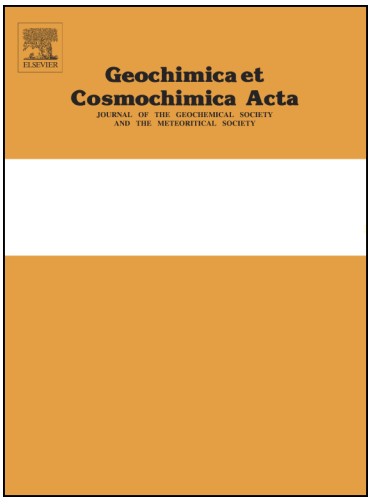

Sorption of rare earth elements onto basaluminite: the role of sulfate and pH

Alba Lozano, Carlos Ayora, Alejandro Fernández-Martínez

PII: S0016-7037(19)30283-2
DOI: https://doi.org/10.1016/j.gca.2019.05.016
Reference: GCA 11242

To appear in: *Geochimica et Cosmochimica Acta*

Received Date: 4 February 2019
Accepted Date: 12 May 2019

Please cite this article as: Lozano, A., Ayora, C., Fernández-Martínez, A., Sorption of rare earth elements onto basaluminite: the role of sulfate and pH, *Geochimica et Cosmochimica Acta* (2019), doi: https://doi.org/10.1016/j.gca.2019.05.016

Sorption of rare earth elements onto basaluminite: the role of sulfate and pH

Alba Lozano[a,b*], Carlos Ayora[a], Alejandro Fernández-Martínez[c]

[a] Institute of Environmental Assessment and Water Research, (IDAEA-CSIC), Jordi Girona 18-26, 08034 Barcelona, Spain

[b] Grup de Mineralogia Aplicada i Geoquímica de Fluids, Departament de Cristal·lografia, Mineralogia i Dipòsits Minerals, Facultat de Geologia, Universitat de Barcelona (UB), C/Martí Franquès, S/N, Barcelona, Spain

[c] Univ. Grenoble Alpes, Univ. Savoie Mont Blanc, CNRS, IRD, IFSTTAR, ISTerre, 38000 Grenoble, France

Corresponding author:

Alba Lozano (alba.lozano@idaea.csic.es)

Abstract

Scandium, yttrium and lanthanides (REE) are critical raw materials in increasing demand for modern technology, so identifying and developing new sources of REE has become a pressing need. REE concentrations in acid mine drainage (AMD) are several orders of magnitude higher than those in natural water, and their recovery is of economic interest. Passive remediation systems designed to minimize AMD impact on the ecosystem retain REE in solid waste, where basaluminite, $Al_4SO_4(OH)_{10}{\cdot}5H_2O$, is the mineral responsible for the scavenge. However, no information about the retention mechanisms of REE is currently available in the literature. The objective of the present work is to study the adsorption of lanthanides, yttrium and scandium onto synthetic basaluminite over a pH range of 4-7 at room conditions. Since sulfate is ubiquitous in AMD, the adsorption has been investigated with variable sulfate concentrations.

Experimental results show that sorption onto basaluminite is strongly dependent on pH, starting at pH 5 for lanthanides and yttrium and at pH 4 for scandium. At any given pH values, sorption increases with sulfate concentration. Distribution coefficients, defined as $K_D = [REE_{sorbed}]/[REE_{solution}]$, are higher for Sc, and across the lanthanide series, the distribution coefficients increase from La to Lu according to decreasing ionic radius, where yttrium is considered close to Ho. Experimental results were modeled using a sorption model that considers mass law equations where the strong sulfate aqueous complex, MSO_4^+, is adsorbed by exchanging a proton with the mineral surface. The dependence of the experimental results on pH suggests the formation of monodentate binding for Y and lanthanides. The bidentate complex for Sc is deduced by the two proton exchange per mol of Sc extracted from the experiments. The thermodynamic constants for the surface complexation reactions were obtained from experiments with high sulfate concentration and were successfully applied to the experiment with low sulfate content and different solid-liquid ratios. Therefore, the model can be applied to interpret the REE geochemistry in natural systems with variable pH and sulfate concentrations.

Keywords

Sorption model, scandium, yttrium, lanthanides, fractionation, sorption edge, non-electrostatic model, monodentate surface species.

1 INTRODUCTION

In the last two decades, there has been an increasing interest in REE, referred to here as the lanthanide series plus yttrium and scandium, due to their high demand in modern industries. The low supply is due to limited REE mining to find new sources of REE (Alonso et al., 2012; Hatch, 2012). Moreover, as a consequence of this industrial activity, new potential pollution sources of REE in natural waters have also emerged (Pagano et al., 2015; Isildar et al., 2018).

Noack et al. (2014) presented a comprehensive study of the REE distribution in groundwater, lakes, rivers and oceans. In particular, REE concentrations in acid mine drainage (AMD) are several orders of magnitude more abundant than other natural water. From the forensic point of view, the REE distribution pattern normalized to the North American Shale Composite (NASC), has been used to prove the impact of Acid Mine Drainage (AMD) in groundwater, rivers and estuarine environments (Delgado et al., 2012; Grawunder et al., 2014; Morgan et al., 2016; Li and Wu, 2017; Bonnail et al., 2017). It is generally recognized that the REE concentration in water is largely controlled by solid surface and aqueous solution chemistry (Quinn et al., 2006a,b and references therein).

REE fractionation between minerals and AMD has been studied since the early 1990s as rock weathering (Auqué et al., 1993, Gimeno et al., 1996) and in mining areas (Gammons et al., 2003). Verplanck et al. (2004) observed REE scavenging from AMD by hydrous ferric oxides as the pH increased to 5.1 due to the water mixing. Similar results were observed by Gammons et al. (2005a,b) when volcanic acidic water mixed with a tributary with neutral pH and the pH increased from 4.3 to 6.1, and when an acidic creek was mixed with a tributary river with circumneutral pH. There, mixtures of ferric and aluminum secondary precipitates were described as being responsible for REE scavenging, yielding Heavy REE (HREE) enrichment in the solids. Similar observations were made by Ferreira da Silva et al. (2009) in the AMD of the Lousal Mine (S. Portugal), where a decrease in REE concentrations was observed as the pH increased from 3 to 6 due to the confluence with a tributary stream. All the aforementioned studies suggested sorption mechanisms on Fe and Al hydroxysulfates as responsible for REE retention. Therefore, interaction with the most relevant solids formed in AMD environments, schwertmannite ($Fe_8O_8(OH)_6SO_4$) and basaluminite ($Al_4SO_4(OH)_{10}·5H_2O$), is expected to play a relevant role in the characteristic water lanthanide distribution pattern.

On the other hand, the treatment of AMD in neutralization plants results in a high amount of sludge made up of schwertmannite and basaluminite. Due to its high water content, the disposal and storage of this waste represents a major operating cost and environmental concern for coal and metal mining operations (Ackman, 1982; Viadero et al., 2006). Similarly, passive mediation systems neutralize AMD by intercepting its natural flux with a permeable filter of limestone (Caraballo et al., 2011). Along this process, sequential precipitation of schwertmannite and basaluminite occurs, causing two well differentiated layers of the solids. Basaluminite retains Sc, Y and lanthanides in the system when it forms at pH values from 4.5 to 6 (Ayora et al., 2016). The REE concentration in basaluminite ranges from 2 to 12 µmol/g, depending on the REE values in the input, and these concentrations are comparable to the grades found in REE deposits and exploration targets (Berger et al., 2009). Despite the fact that schwertmannite precipitates before basaluminite (from pH 3-3.5), it does not retain REE.

Therefore, a detailed understanding of the mechanism responsible for selective REE scavenging is necessary.

Currently, most REE sorption and fractionation studies have focused on hydrous ferric and manganese oxides in marine water (Byrne and Kim, 1990; Bau et al., 1996) and interactions between synthetic marine water and manganese and ferric oxides (Koeppenkastrop and De Carlo, 1992; Pourret and Davranche, 2013). Differences in solid origin and water source result in distinct fractionation. Light REE (LREE) enrichments were observed in silica phases (Byrne and Kim 1990) as well as in synthetic MnO_2 and α-FeOOH solids (Koeppenkastrop and De Carlo, 1992). In contrast, HREE enrichment was observed in synthetic FeOOH and MnO_2 (De Carlo et al., 1998) as well as hydrogenetic Mn-Fe crusts (Bau et al., 1996). With application to continental water, Liu et al. (2017) developed a surface complexation model (SCM) to interpret REE sorption in iron hydroxide. Additionally, other studies focused on REE interaction with organic matter and its affection with the organic acids of soils (Tang and Johannesson 2003; Verplanck et al., 2004; Pourret and Martinez, 2009).

Aluminum phases are not as common as ferrous oxide phases, and there are few studies related to the REE uptake for aluminum oxides. For example, the uptake of Eu and Yb by alumina (Al_2O_3) at varying pH has been studied by soil scientists as an analogue for actinides in nuclear waste disposal. Experimental sorption edges for Yb and Eu(III) onto alumina were reproduced by Marmier et al. (1997) and Rabung et al. (2000), respectively, using an SCM. In all of the studies, the REE sorption is dependent on pH.

In addition to pH, sulfate has the potential to change the sorption behavior of REE and other metals in AMD systems. Indeed, aqueous sulfate complexes are predominant in AMD over a wide range of pH values (Gimeno et al., 2000), and sulfate is a major constituent of the Fe and Al solid phases, schwertmannite and basaluminite. Therefore, sulfate is expected to play a major role in aqueous-solid partitioning. Despite their key role in AMD geochemistry, no experimental or modeling studies of REE sorption for these two minerals have been investigated. In this study, we present experimental results for adsorption of REE onto synthetic basaluminite as a function of pH and two different sulfate concentrations. To understand the REE sorption mechanism onto basaluminite, a surface complexation model is proposed from a sorption experiment with sulfate and subsequently validated with a second experiment at very low sulfate concentration.

2 Materials and methods

2.1 Experimental part

2.1.1 Preparation and characterization of synthetic basaluminite

Basaluminite was synthesized following the method described by Adams and Rawajfih (1977) by adding 214 mL of 0.015 M $Ca(OH)_2$ to 30 mL of 0.05 M $Al_2(SO_4)_3 \cdot 18H_2O$; both commercial reagents. The resulting solid was washed several times with Milli-Q water to remove the coprecipitated gypsum, and dried for 2 days at 40°C. As shown by X-ray diffraction (XRD), the resulting solid was free of impurities (Fig. SI-1).

The specific surface area was obtained by the BET-N_2 sorption method, using a Micromeritics Gemini V analyzer. The sorption site density was calculated based from the crystal structure of felsöbanyáite, with a local order similar to that of basaluminite (Farkas and Pertlik, 1997; Carrero et al., 2017).

2.1.2 REE sorption as function of pH and sulfate

Two sets of batch experiments were performed to study the SO_4 dependence of REE adsorption onto synthetic basaluminite as a function of pH: low and high sulfate concentration. Two stock solutions were prepared from an ICP standard mix (Merck) of 16 elements –excluding Pm- with Milli-Q water (the total REE in the stock solution was 123.3 µM). The first stock solution consisted of 1 mg/L of each REE, whereas the second stock solution contained 1mg/L of each REE plus 20 mg/L Na_2SO_4. The initial pH of the stock solutions was 2.5. A sequence of 10 mL aliquots of each stock solution were adjusted to a desired pH range of 4.5-7 via addition of a 0.05 M NH_4OH solution. The first set of experiments was carried out by adding 10 mg of synthetic basaluminite to each aliquot of the first stock solution. Despite aqueous sulfate is initially absent, this set of experiments will hereafter be referred to as a low sulfate (0.5 mM SO_4) due to the release of small amounts of sulfate adsorbed in the synthesis of basaluminite (see chapter 3.2). The second set of experiments was similar to the first one, but using the second stock solution (20 mM SO_4). Finally, a third set of batch experiments with a different solid:liquid ratio was performed to test the validity of the model developed. It consisted of suspensions of 10 mg of synthetic basaluminite in 40 mL of the second stock solution (20 mM SO_4).

The solid was added to each solution and the suspensions were shaken for 6 hours at room temperature. Previous kinetic experiments were performed at pH 6-6.5, and maximum adsorption was reached at 6 hours and continued from there on. Similar results were obtained by Koeppenksastrop and De Carlo (1992) with fast REE adsorption onto MnO_2, hydroxyapatite and goethite and amorphous FeOOH, reaching an uptake of 60-90% of the initial dissolved REE in 4 hours. Due to basaluminite instability (Lozano et al., 2018), equilibrium times longer than 6 hours were not used. Each pH was readjusted to the initial value after basaluminite addition because the pH drops when the mineral exchanges SO_4 with OH. Once the experiment finished, the suspensions were centrifuged for 15 min at 4500 rpm (4150 RCF). The supernatant was filtered through 0.22 µm nylon membranes into test tubes. The filtered supernatant samples were diluted fivefold with 1% HNO_3. The REE concentrations in the solutions were determined by ICP-MS. Raw data from each experiment were corrected by a

dilution factor based on the amount of NH_4OH added. The solids were dried at 40°C for 48 h. The reproducibility of the experiments was determined by replication at pH 6.7. The error of the final pH values was ± 0.02. The sorbed fractions were calculated as follows:

$$\text{Sorbed fraction} = \frac{[\text{REE}]_{\text{initial}} - [\text{REE}]_{\text{final}}}{[\text{REE}]_{\text{initial}}} \quad (1)$$

where [REE] is the concentration of each REE. Initial concentration was measured from stock solution and final concentration in each different batch after experiment. The distribution coefficients K_D (L/kg) were calculated from the REE sorbed onto the solid per the concentration of REE remained in solution and normalized per volume of solution and mass of solid (solid to liquid ratio):

$$K_D = \frac{[\text{REE}]_{\text{initial}} - [\text{REE}]_{\text{final}}}{[\text{REE}]_{\text{final}}} \cdot \frac{V_{\text{solution}}}{M_{\text{solid}}} \quad (2)$$

2.1.3 Analytical techniques

Measurements of pH values from filtered aliquots were made with a Crison® glass electrode calibrated with buffer solutions of pH 2, 4, 7 and 9. Major cation (S, Al, and Na) concentrations were measured by ICP-AES (Thermo Scientific – iCAP 6500, Radial acquisition) and REE (La,Ce, Pr, Nd, Sm, Eu, Gd, Tb, Dy, Ho, Er, Tm, Yb, Lu, Y and Sc) were determined with ICP-MS (Perkin-Elmer®SciexElan 6000). The detection limits were 1.6, 1.0 and 4.3 µmol/L for S, Al and Na, respectively, and 0.2 µg/L for REE. The analytical precision error was estimated to be approximately 5% for ICP-AES and 2% for ICP-MS measurements. Certified solutions (CPI International-CCV standard 1-solution A) and two AMD laboratory standards supplied by P. Verplanck (USGS), were intercalated within the samples to check the analytical accuracy. The deviation from the recommended values was always lower than 5%, with the exception of Eu, giving values 20% below the value reported by Verplanck et al. (2001).

The solid phase prior and after the sorption experiments was investigated by High Energy X-ray Diffraction (HEXD) at the ID31 beamline at the European Synchrotron Radiation Facility (ESRF).

2.2 REE speciation

Chemical speciation of dissolved REE and surface complexation modeling was calculated by PHREEQC code (Parkhurst and Appelo, 1999) using the database of Donnee Thermoddem_V1.10 (Blanc et al., 2012). The database has been updated with the stability constants at zero ionic strength and 25°C for the following inorganic complexes for lanthanides and yttrium (M): MCO_3^+, $M(CO_3)_2^-$ and $MHCO_3^{2+}$ (Luo and Byrne, 2004); MSO_4^+ (Schijf and Byrne, 2004); MOH^{2+} (Klungness and Byrne, 2000), $M(OH)_2^+$, $M(OH)_3^0$ (Lee and Byrne, 1992); MCl^{2+} (Luo and Byrne, 2001); MF^{2+}, MF_2^+ (Luo and Millero, 2004); and MNO_3^{2+} (Millero, 1992). Solubility products for REE solids, $M(OH)_3$ and $M(OH)_3$(am), were added from LLNL database (Johnson et al., 2000) database and Spahiu and Bruno (1995). Scandium aqueous complexes, $Sc(OH)^{2+}$, $Sc(OH)_2^+$, $Sc(OH)_3^0$, $ScSO_4^+$; and the solubility product for $Sc(OH)_3$ by Wood and Samson (2006) were also added to Donnee Thermoddem_V1.10 database. Equilibrium constants for aqueous species are compiled in Table SI-1 of Supporting Information.

3 RESULTS

3.1 Basaluminite characterization

The BET method measured a specific surface area of 68 m^2/g. The potentiometric titrations of synthetic basaluminite have been attempted at three different ionic strengths, 0.1, 0.02 and 0.005 M of $NaNO_3$. However, the mineral is proved to release sulfate and transform into nanoboehmite as OH^- is incorporated to the solution (Lozano et al., 2018). This behavior prevented the acquisition of consistent titration curves and their prediction with current electrostatic models. Therefore, the surface properties could not be obtained. Then, the site densities were calculated from crystal structure of felsöbányaite, as basaluminite presents similar local order, as stated by Farkas and Pertlik (1997) and Carrero et al. (2017). The single coordinate sites (one oxygen atom linked to one Al atom) calculated were 4.94, 4.24 and 4.70 nm^{-2} for the 100, 010 and 001 faces, respectively, (5.5 sites/112.32 $Å^2$ for (100), 6.25/147.38^2 for (010) and 6.25/132.80^2 for (001)) from the unit cell of basaluminite, with a space group of P_21. The average surface site is 4.60 nm^{-2} (see Fig. SI-2 for structural details).

3.2 REE adsorption as a function of pH and sulfate

The chemical compositions of the initial and final solutions of the two sets of experiments with 1 g/L of solid:liquid ratio are compiled in Table SI-2. All final solutions were subsaturated with respect to the REE hydroxides (Table SI-3), and, therefore, no REE hydroxide precipitation was expected. All the final solutions except one were supersaturated with respect to basaluminite (Saturation indices between 0.06 and 1.3).

Small amounts of dissolved sulfate were present in the final solutions without initial sulfate. There, the amount of dissolved sulfate increased from 0.1 to 0.9 mM with increasing pH. This is interpreted as the exchange of sulfate from basaluminite with OH groups from the solution (Lozano et al., 2018). The experiments without initial sulfate will be hereafter noted as 0.5 mM SO_4, indicating the mean value.

Four elements were selected for representation: La as light REE (LREE), Lu as heavy REE (HREE), Sc and Y. The two sets of sorption experiments with different sulfate concentrations showed increasing REE sorption with pH (Fig. 1). The adsorption edges occur over a range of 2.0 to 2.5 pH units. Lanthanides and yttrium sorption became significant at pH 5. However, the pH values at which different REE are sorbed differ for each element. The sorption edges shifted to lower pH values for HREE with respect to LREE, and preferential sorption of HREE over LREE was observed. Scandium behaved differently, being scavenged at pH values considerably lower than the rest, and sorption of Sc became significant at pH 4. Similar pH dependence was observed in the experiment with 0.25 g/L of solid:liquid ratio. As expected, the sorption edges are shifter to higher pH values (Table SI-4), as it will be commented in section 4.3.

The sulfate dependence of REE sorption is more evident by plotting the results of both experiments together by element (Fig. 2). REE sorption is greater when sulfate is present in solution along the entire pH range studied. Sorption enhancement varies with the pH range for each element. For instance, at pH 5.4 the sorption fraction for the higher sulfate in solution is 0.2 points higher for Lu, 0.1 points for Y, 0.1 for Sc and 0.05 for La. This enhancement increases at pH 6: for Lu (0.3 points higher) and for Y (0.2 points) but decreases for Sc (0.05) and for La,

which has the same sorbed fraction. The effect for the enhancement of REE sorption with higher sulfate concentration has also been observed for other trace metal sorption, such as Cu and Pb, onto ferrihydrite and schwertmannite (Webster et al., 1998; Baleeiro et al., 2018). Webster et al. (1998) concluded that the enhanced sorption of Cu onto iron (III) oxy-hydroxy sulfate observed with higher sulfate in solution was due to the formation of ternary complexes with a ferric surface site, e.g., $\equiv FeOHCuSO_4$. Similarly, Baleeiro et al. (2018) pointed out that these kinds of ternary surface complexes could explain the strong affinity of these trace metals with schwertmannite.

Values for the distribution coefficient (K_D) were calculated by Eq. (2) and are presented for the lanthanide series in Fig. 3. At pH values lower than 5, the distribution patterns are almost flat and from pH 5 upwards, when the sorbed fraction is significant, log K_D patterns reflect HREE enrichment relative to LREE in the solid phase (Fig. 3), varying 1 unit of log K_D along the series in both sets of experiments. Similar patterns were observed by Bau 1999 for their coprecipitation experiments of REE and Fe at low pH values. Similar relative enrichment in heavy lanthanides was observed in aluminum and ferric hydroxides precipitated in acidic rivers after their neutralization via mixing with alkaline tributaries (Gammons et al. 2003, 2005; Verplanck et al., 2004). Similar to those described by Masuda et al. (1987) and Bau (1996), the fractionation patterns showed an M-type tetrad effect (where they can be subdivided into four convex segments: from La to Nd, from Nd to Gd, from Gd to Ho and from Ho to Lu (Fig. 3). A small positive Ce anomaly was observed only at low pH and low SO_4 concentration, possibly due to a partial/total oxidation of Ce^{3+} to Ce^{4+}, as Koeppenkastrop and De Carlo (1992) proposed for the positive anomalies observed in vernadite. Yttrium has a similar ionic radius as Dy and Ho and can be placed between them (not shown in the figure). For the different pH values represented in Fig. 3, the log K_D patterns show a negative Y anomaly. This anomaly is expressed in K_D^Y/K_D^{Dy} and K_D^Y/K_D^{Ho} ratios below unity, which is observed along the pH range for both sets of experiments with 20 and 0.5 mM sulfate concentration (Table SI-5). In the experiments with low SO_4 concentration, Yb and Dy displayed negative anomalies that attenuated as the pH increased. These anomalies were absent at high sulfate concentrations. In contrast, at higher sulfate concentrations, Er showed a negative anomaly at lower pH values that was attenuated when pH increased and this Er anomaly was not observed with lower sulfate content. These anomalies are not previously described in similar sorption/coprecipitation experiments using amorphous ferric hydroxides (Bau, 1999; Ohta and Kawabe, 2000a; Quinn et al., 2006a).

4 Discussion

4.1 Aqueous speciation

The presence of sulfate in the solution affects the REE aqueous speciation since it strongly complexes with REE (Gimeno et al., 2000). The proportion of sulfate complexes increases with sulfate concentration and becomes predominant for SO_4 concentrations higher than 1 mM. The rest of the aqueous complexes, MOH^{2+}, MCO_3^+ and $M(CO_3)_2^-$ are only significant at pH values higher than 6.5 and low SO_4 concentrations, as represented for Y in Fig. 4A,B and extended for the rest of lanthanides. Scandium speciation differs from the rest, where Sc hydrolysis complexes are also significant at pH values higher than 4.6 (Fig. 4C,D). For Sc, there

is no information about the carbonate complexation in the literature (Wood and Samson 2006), possibly because $ScCO_3^+$ formation is not thermodynamically favorable compared to the formation of strong hydrolysis products.

4.2 Model description

Surface Complexation Models (SCM) are commonly referred to as providing chemical and molecular descriptions of adsorption using equilibrium thermodynamics that can be applied to different conditions (Goldberg, 1992). The common characteristics of these models are the surface charge balance, electrostatic potential terms, as an effect of surface charge, and several adjustable parameters: equilibrium constants, total number of reactive sites and capacitance density.

In a non-electrostatic model (NEM), the electrostatic term is ruled out when the chemical interaction of the cations adsorption is stronger than electrostatic forces in the sorption process (Davis and Kent, 1990). For REE in particular, several works model the sorption experimental data with NEM, and thus, discard the electrostatic term. Marmier and Fromage (1999) reported a non-electrostatic surface complexation model to describe the sorption of lanthanum in hematite. Tertre et al., 2008 described a non-electrostatic model for REE adsorption on basaltic rock. Rabung et al., (2000) and Quinn et al., (2006a,b) also described a sorption model for Y and lanthanides in amorphous iron hydroxides without taking into account the electrostatic term. In our case, the metaestable character of the mineral precluded the full determination of basaluminite surface properties and thus, a non-electrostatic model will be used.

On the other hand, models proposed for REE sorption on amorphous ferric and manganese oxides, hematite, goethite, aluminum hydroxide and alumina are traditionally explained by the sorption of free ions onto surface sites (Tochiyama et al., 1996, Rabung et al., 1998; Marmier et al., 1997; Marmier and Fromage 1999; Quinn et al., 2006a). In the present work, owing to the predominance of sulfate complexes in the aqueous phase, the experiments were initially modeled by the reaction of the aqueous sulfate complex MSO_4^+ with surface sites. This result is consistent with the observation of higher adsorption in the experiments with the SO_4-rich solutions (20 mM). In the case of Sc, in addition to $ScSO_4^+$, the aqueous speciation showed a higher stability of the hydrolysis species $Sc(OH)^{2+}$ in the experiments with lower sulfate concentration (Fig. 4C,D), and the sorption of this aqueous species was also considered. Although experiments were conducted at room conditions, carbonate complexation has not been considered experimentally since the proportion of carbonate species is very low at the experimental pH range (Fig. 4).

The sorption reaction is proposed as the exchange of the M^{z+} aqueous complex (M^{z+} accounting for MSO_4^+ and $Sc(OH)^{2+}$) with n protons from n surface sites represented by XOH:

$$M^{z+} + nXOH = (XO)_n M^{z-n} + nH^+ \qquad K_M \tag{3}$$

The equilibrium constant K_M of the reaction for each REE (M) would be:

$$K_M = \frac{\{(XO)_n M^{z-n}\} \cdot a_{H^+}^n}{a_{M^{z+}} \{XOH\}^n} \tag{4}$$

where a_{Mz+} and a_{H+} are the activities of the aqueous complex and proton, respectively; and $\{(XO)_nM^{z-n}\}$ and {XOH} account for the mole fraction of the sorbed species ($[(XO)_nM^{z-n}]/[T_{XOH}]$) and the free surface sites ($[XOH]/T_{XOH}$), respectively.

A total surface site concentration T_{XOH} of 516 µmol/kg was obtained from the basaluminite site density of 4.6 site/nm^{-2}, the specific surface area of 68 m^2/g. The concentration of free surface sites was calculated as:

$$[XOH] = T_{XOH} - \sum n\,[(XO)_nM^{z-n}] \quad (5)$$

The value of the equilibrium constant K_M for each element was obtained with data from the experiment with 20 mM SO_4, except for the case of the species $Sc(OH)^{2+}$, which was obtained from the experiment with 0.5 mM SO_4.

Thus, replacing the molar fraction by their values, taking logarithms of Eq. (4) and rearranging the order we obtain a linear expression (Eq.6):

$$\log \frac{[(XO)_n M^{z-n}]}{a_{Mz+}} \log = \log K_M + n\,pH + n \log[XOH] - (n-1)\log T_{XOH} \quad (6)$$

For low occupancy of surface sites, [XOH] and T_{XOH} are practically coincident and Eq. 6 can be approximated as:

$$\log \frac{[(XO)_n M^{z-n}]}{a_{Mz+}} = \log K_M + n\,pH + \log T_{XOH} \quad (7)$$

Therefore, the equilibrium constants determined here ($K_M \cdot T_{XOH}$) are those referred to as the K_3 according to the model 3 proposed by Wang and Giammar (2013).

By plotting the experimental data according to Eq. (6), linear correlations were obtained. Except for Sc, the slope of the regression was close to 1, where only La showed a slope value below 1. For the rest of lanthanides, the slopes were higher than 1 and increased progressively from LREE to HREE, reaching up to 1.3 (Fig. 5). A slope close to 1 suggests that the sorption occurs as a monodentate complex as indicated by the Eq. 3 (Rabung et al., 1998 and 2000). Similar observations were obtained by Rabung et al. (2006), after fitting EXAFS spectra of a γ-Al_2O_3 sorbed with Lu, where Lu formed a monodentate inner sphere complex.

Unlike Y and the lanthanides, the log K_D-pH regression for $ScSO_4^+$ data from the 20 mM SO_4 experiment resulted in a slope close to 2 (2.37) (Fig. 6A). Similar results were observed for $Sc(OH)^{2+}$ with a slope of 1.90 from the experiment with 0.5 mM SO_4, where it was the major species (Fig. 6B). In both cases, a slope of 2 suggests exchange with two surface protons and formation of a bidentate surface complex for both aqueous species. Despite the fact that $Sc(OH)_2^+$ was predominant at pH 5.5, this aqueous species provided a very low slope and poorer correlation (not shown), and was not considered a sorbed species.

To obtain surface sorption constants, the regression slopes were forced to 1 for yttrium and lanthanides and to 2 for Sc via the Gnuplot v5.00 software (Williams and Kelley, 1986) using experimental data with higher sulfate content in solution. The resulting log K_M was obtained as the intercept. The error of the regression calculation was larger and enclosed the analytical error, and it was assumed to be the error of the log K_M value. The log K_M values and the

regression errors for surface complexation reactions for all REE are listed in Table 1. Apart from values for Sc complexation, the equilibrium constants increased from -2.48 to -2.19 from La to Lu, indicating higher HREE than LREE affinity for the basaluminite surface. These log K_M values are close to those obtained by Quinn et al. (2006a) for complexation of free REE ions onto ferric oxide surfaces.

4.3 Validation

Log K_M values conducted at high sulfate concentration (as above) were validated with results from the experiment with lower sulfate content. In the case of Sc, the log K_M of reaction (6), obtained from the experiments with low sulfate content, was used to predict of the sorption edge curves for the 20 mM SO_4 experiment. The model results are plotted with continuous lines in Fig. 7. Model results for each REE are plotted in Figs. SI-3 and SI-4.

A temperature of 25°C and a pCO_2 of 3.5 was considered to reproduce room conditions in the sorption models. At higher pH values than 6.5 a mismatch between the modeled sorbed fractions (solid lines in Fig. 7) and the experimental ones (symbols) for the experiment with the lower sulfate content is attributed to the presence of dissolved carbonate species. Thus, MCO_3^+ species form and take part in the sorption process. To show the possible role of carbonate complexes at pH higher than 6.5 and low sulfate concentration, the sorption of MCO_3^+ complexes has been included in the model. The equilibrium constants for the MCO_3^+ sorption reactions have been recalculated from those reported by Quinn et al. (2006b) for goethite (Table SI-6). Including carbonate complexation, the model predicts sorption at near neutral pH when lower sulfate is present in solution, supporting the role of carbonate complexation at such particular conditions (pointed lines in Fig. 7).

As expected, the model reproduces the sorption edges in the experiment with 20 mM SO_4 (Fig. 7, left) well. Indeed, only adsorption very close or outside the experimental error is predicted for La and Ce at some pH values below 6.0. Although worse, the model for the experiment with lower sulfate content is also acceptable, and the predicted values in general fit the analyses within experimental error (Fig. 7, right). A slight overprediction of the adsorption at intermediate pH values and an underprediction at high pH values is systematically observed.

In addition to the sorption edges, the model also predicted the fractionation patterns of the lanthanide group (Fig. SI-5) and the M-type tetrad effect, within experimental error. As observed in the pH sorption edge curves, the model tends to underpredict the K_D values at pH 6.4. This is especially relevant for low sulfate concentration (Fig. SI-5B) and is attributed to the increasing importance of MCO_3^+ aqueous complexes at near neutral pH. In contrast, the model tends to overpredict the values for the intermediate pH (between 5.5 and 6.5), particularly for the intermediate lanthanides. The yttrium experimental K_D values are well predicted in all cases. However, the model fails to predict other anomalies. For instance, the positive Ce anomaly observed at pH values lower than 5.3 in the experiment without an initial sulfate concentration is not reproduced. Similar observations were described in Bau (1999) for REE scavenged in Fe oxyhydroxide at a pH lower than 5 and were attributed to a partial oxidation of Ce(III) at low pH. Similar poor fit was observed for the Er negative anomaly in sorption with high sulfate in solution and, the Dy and Yb negative anomalies detected with lower aqueous sulfate concentrations were not predicted by the model. In the latter case, no previous

descriptions of these anomalies have been reported and they might be related to an analytical error for very low concentration.

The good fit between the predicted and measured Sc values confirms a good model prediction as bidentate for this element. As observed in Fig. 7, the $(XO)_2ScSO_4^-$ complex predominates in the experiment with 20 mM SO_4, and the $(XO)_2ScOH$ complex predominates in the experiment with a low SO_4 concentration. Again, Sc behaves differently due to the stronger hydrolysis effect than sulfate complexation. The higher ligand ratio for Sc may be due to its structural characteristics. Lanthanide cations are larger than Sc^{3+}, and have coordination numbers ranging from 8 (with a tricaped trigonal prism configuration) to 9 (with a distorted square antiprism or dodecahedron configuration of the hydration sphere) (Lindqvist-Reis et al., 2000; Rouse et al., 2001). On the contrary, Sc^{3+} (0.75 Å) has an ionic radius closer to that of Al^{3+} (0.53 Å), adopting an octahedral coordination (Lindqvist-Reis et al., 2006; Levard et al., 2018). This fact leads to similar interatomic distances to oxygen, allowing the formation of complexes with bidentate ligands. The different behavior of Sc suggests its potential segregation from the rest of the REE.

Finally, the model was also tested with experimental data for a solid:liquid ratio of 0.25 g/L. The results for four selected elements are included in Fig. 8 (the results for the initial ratio of 1 g/L are also included). The comparison between predicted and experimental values for the complete set of REE is in Fig. SI-6. As expected, the model predicts lower adsorption for lower solid:liquid ratio, showing a general consistency with experimental data. Comparing the prediction along the lanthanide series with experimental sorption data, the model better predicts HREE than LREE, where the predicted sorption was slightly lower than observed for La, Ce and Pr. Interestingly, Sc sorption by means of bidentate complexes was satisfactory predicted.

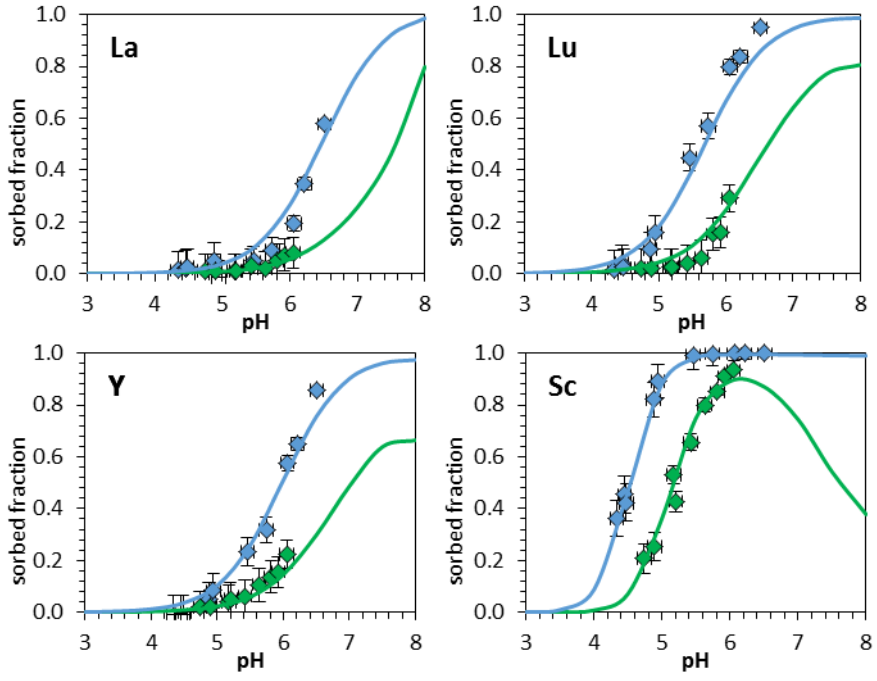

Fig. 8. Comparison between experimental data (symbols) and calculated fraction (lines of the sorption edge curves for Sc, Y, La and Lu at two different solid:liquid ratios (1 g/L the blue

symbols and 0.25 g/L the green ones) and 20 mM SO_4. Calculations at 25°C and pCO_2 of 3.5, including the carbonate complexation constants listed in Table SI-6.

5 CONCLUSIONS

This work shows that basaluminite has a high capacity to retain REE by an adsorption mechanism, and this process is highly dependent on pH. Thus, REE sorption on basaluminite starts to be significant between pH 5-5.5 for lanthanides and yttrium and from pH 4-4.5 for Sc, depending on the solid:liquid ratio. Lanthanide fractionation also occurred from pH 5.3, yielding the M-type tetrad effect and reflecting HREE enrichment onto the solid. These results are analogous to the fractionation observed in Al and Fe oxide precipitates in the confluence of acid sulfate waters with natural streams and rivers and therefore could explain the mechanism of REE retention in natural precipitates. As expected from the overwhelming importance of the sulfate aqueous speciation (MSO_4^+), higher REE sorption was observed at higher sulfate concentrations. These results confirm that aqueous speciation and sorption onto basaluminite control the REE geochemistry in acid rock/mine drainages.

A non-electrostatic surface complexation model has been proposed to explain the sorption mechanism. In the model description, sulfate plays a key role since the strong complexation with REE leads to sorption of the aqueous sulfate complex MSO_4^+, rather than the free ion M^{3+}, as commonly described by other authors for REE sorption in oxides. Thanks to experimental data from the REE sorption experiment with high sulfate concentration (20 mM), surface constants were calculated and validated with experiments with low sulfate concentration (0.1 to 0.9 mM) and a lower solid:liquid ratio. Additionally, at near neutral pH and sulfate concentrations lower than 1 mM, the sorption of the aqueous carbonate complex, MCO_3^+, should be considered when mixing with natural water.

This work presents for the first time sorption equilibrium constants for REE sorption onto basaluminite, a very common mineral in mine discharge. Despite REE behaving as a group with similar chemical properties and forming monodentate complexes, their ionic radii variy along the series, and the different distances lead to slightly different positions on the basaluminite surface. This is clearly observed with Sc, with a considerably smaller ionic radius than the other REE, which forms bidentate surface links. Additionally, its aqueous speciation, with the formation of stable hydroxyl species, makes Sc behave differently from the other REE and sorb at lower pH values. This knowledge could help design REE separation mechanisms and isolate cost-effective elements.

Acknowledgements

This work was funded by the European EIT 'Morerecovery' and the Spanish SCYRE (CGL2016-78783-C2-R)] projects. A. L. was also funded by the FPI grant (BES-2014-069978). The authors wish to thank J. Bellés, M. Cabañas, R. Bartrolí and N. Moreno (IDAEA-CSIC) for their analytical assistance. The manuscript has been greatly improved with the comments of Prof. Villalobos and three anonymous reviewers.

References

Ackman, T. (1982) Sludge disposal from acid mine drainage treatment. *Report of Investigation 8672*. US Bureau of Mines, Pittsburgh.

Adams F. and Rawajfih Z. (1977) Basaluminite and alunite: a possible cause of sulfate retention by acid soils. *Soil Sci. Soc. Am. J.* **41**, 686–692.

Alonso, E., Sherman, A. M., Wallington, T. J., Everson, M. P., Field, F. R., Roth, R., Kirchain, R. E. (2012) Evaluating Rare Earth Element availability: A Case with revolutionary demand from clean technologies. *Environ. Sci. Technol.* **46**, 3406−3414.

Auqué L. F., Tena J.M., Gimeno M. J., Mandado J. M., Zamora A., Lopez-Julian P.L. (1993) Distribución de tierras raras en soluciones y coloides de un sistema natural de aguas acidas (Arroyo del Val, Zaragoza). *Est. Geol.* **49**, 41–48.

Ayora C., Macías F., Torres E., Lozano A., Carrero S., Nieto J. M., Pérez-López R. Fernández-Martínez A. and Castillo-Michel H. (2016) Recovery of rare earth elements and yttrium from passive-remediation systems of acid mine drainage. *Environ. Sci. Technol.* **50** (15), 8255-8262.

Baleeiro, A., Fiol, S., Otero-Fariña, A., Antelo, J. (2018) Surface Chemistry of Iron Oxides Formed by Neutralization of Acidic Mine Waters: Removal of Trace Metals. *Appl. Geochemistry* **89**, 129–137.

Bau M., Koschinsky A., Dulski P. and Hein J. R. (1996) Comparison of the partitioning behaviours of yttrium, rare earth elements, and titanium between hydrogenetic marine ferromanganese crusts and seawater. *Geochim. Cosmochim. Acta* **60**, 1709–1725.

Bau M. (1999) Scavenging of dissolved yttrium and rare earths by precipitating iron oxyhydroxide: experimental evidence for Ce oxidation, Y–Ho fractionation, and lanthanide tetrad effect. *Geochim. Cosmochim. Acta* **63**, 67–77.

Berger, V. I.; Singer, D. A. and Orris, G. J. (2009) Carbonatites of the world: explored deposits of Nb and REY. Database and grade and tonnage models. *USGS Open-File Repor*t, 11-39.

Blanc Ph., Lassin A., Piantone P., Azaroual M., Jacquemet N., Fabbri A., and Gaucher E.C. (2012) Thermoddem: Ageochemical database focused on low temperature water/rock interactions and waste materials. *App. Geochem*. **27**, 2107-2116.

Bonnail, E.; Pérez-López, R.; Sarmiento, A. M.; Nieto, J. M.; DelValls, T. Á. A (2017) Novel approach for acid mine drainage pollution biomonitoring using rare earth elements bioaccumulated in the freshwater clam Corbicula fluminea. *J. Hazard. Mater.* **338**, 466–471.

Byrne, R. H. and Kim, K. H. (1990) Rare earth element scavenging in seawater. *Geochim. Cosmochim. Acta* **54**, 2645-2656.

Caraballo, M. A.; Macías, F.; Rötting, T. S.; Nieto, J. M.; Ayora, C. (2011) Long term Remediation of highly polluted acid mine drainage: A sustainable approach to restore the environmental quality of the Odiel river basin. *Environ. Pollut.* **159** (12), 3613–3619.

Carrero S., Fernández-Martínez A., Pérez-López R., Lee D., Aquilanti G., Poulain A., Lozano A. and Nieto J. M. (2017) The nanocrystalline structure of basaluminite, an aluminum hydroxide sulfate from acid mine drainage. *Am. Mineral*. **102**, 2381-2389

Davis, J. A., Kent, D. B. (1990) Surface Complexation Modeling in Aqueous Geochemistry. Vol. 23, pp 177–260.

De Carlo E. H., Wen X. and Irving M. (1998) The influence of redox reactions on the uptake of dissolved Ce by suspended Fe and Mn oxide particles. *Aquat. Geochem.* **3**, 357–389.

Delgado, J.; Pérez-López, R.; Galván, L.; Nieto, J. M.; Boski, T. (2012) Enrichment of rare earth elements as environmental tracers of contamination by acid mine drainage in salt marshes: A new perspective. *Mar. Pollut. Bull.* **64** (9), 1799–1808.

Farkas, L. and Pertlik, F., (1997) Crystal structure determinations of felsöbányaite and basaluminite, Al4(SO4)(OH)10·4H2O. *Acta Mineral.-Petrogr. Szeged* **38**, 5–15.

Ferreira da Silva, E.; Ferreira, E. ; Bobos, I; Matos, J.; Patinha, C.; Reis, A. P.; Fonseca, E. C. (2009) Mineralogy and geochemistry of trace metals and REE in massive volcanic sulphide host rocks, stream sediments, stream waters and acid mine drainage from the Lousal mine area (Iberian Pyrite Belt, Portugal). *Appl. Geochem*. **24**, 383-401.

Gammons C. H., Wood S. A., Jonas J. P., and Madison J. P. (2003) Geochemistry of rare earth elements and uranium in the acidic Berkeley Pit lake, Butte, Montana. *Chem. Geol*. **198**, 269–288.

Gammons, C. H.; Wood, S. A.; Nimick, D. A. (2005a) Diel behavior of rare earth elements in a mountain stream with acidic to neutral pH. *Geochim. Cosmochim. Acta* **69** (15), 3747–3758.

Gammons C. H., Wood S. A., Pedrozo F., Varekamp J. C., Nelson B. J., Shope C. L. and Baffico G. (2005b) Hydrogeochemistry and rare earth element behavior in a volcanically acidified watershed in Patagonia, Argentina. *Chem. Geol*. **222**, 249−267.

Gimeno, M.J., Auque, L.F., Lopez-Julian, P.L., Gomez-Jime- nez, J., Mandado, J.M. (1996) Pautas de distribución de especies de las tierras raras en soluciones ácidas naturales. *Est. Geol*. **52**, 11–22.

Gimeno, M.J., Auque, L.F., Nordstrom D.K. (2000) REE speciation in low-temperature acidic waters and the competitive effects of aluminum. *Chem. Geol*. **165**, 167–180.

Goldberg, S. (1992) Use of surface complexation models in soil chemical systems. *Adv. Agron.* **47**, pp 233–329.

Grawunder, A., Merten, D.;,Büchel, G. (2014) Origin of middle rare earth element enrichment in acid mine drainage-impacted areas. *Environ. Sci. Pollut. Res.*, *21* (11), 6812–6823.

Hatch, G. P. (2012) Dynamics in the global market for rare earths. *Elements* **8,** 341-346.

Isildar A., Rene E.R.; van Hullenbusch E.D.; Lens P.N.L. (2018) Electronic waste as a secondary source of critical metals: Management and recovery technologies. *Resour. Conserv. Recycl*. **135**, 296-312.

Klungness G. D. and Byrne R. H. (2000) Comparative hydrolysis behavior of the rare earths and yttrium: the influence of temperature and ionic strength. *Polyhedron* **19**, 99–107.

Koeppenkastrop D. and De Carlo E. H. (1992) Sorption of rare- earth elements from seawater onto synthetic mineral particles: an experimental approach. *Chem. Geol.* **95**, 251–263.

Lee, J.H., Byrne, R.H. (1992) Examination of comparative rare earth element complexation behavior using linear free-energy relationships. *Geochim. Cosmochim. Acta* **56**, 1127–1137.

Levard, C.; Borschneck, D.; Grauby, O.; Rose, J.; Ambrosi, J.-P. (2018) Goethite, a tailor-made host for the critical metal scandium: The $Fe_xSc_{(1-x)}OOH$ solid solution. *Geochemical Perspect. Lett.* **9**, 16–20.

Li, X.; Wu, P. (2017) Geochemical characteristics of dissolved rare earth elements in acid mine drainage from abandoned high-As coal mining area, southwestern China. *Environ. Sci. Pollut. Res.* **24** (25), 20540–20555.

Lindqvist-Reis, P.; Lambe, K.; Pattanaik, S.; Persson, I.; Sandström, M. (2000) Hydration of the Yttrium(III) ion in aqueous solution . An X-ray diffraction and XAFS structural study. *J. Phys. Chem. B* **104,** 402–408.

Lindqvist-Reis, P.; Persson, I.; Sandström, M. (2006) The hydration of the Scandium(III) ion in aqueous solution and crystalline hydrates studied by XAFS spectroscopy, large-angle X-ray scattering and crystallography. *Dalt. Trans.* **32**, 3868–3878.

Liu, H.; Pourret, O.; Guo, H.; Bonhoure, J. (2017) Rare earth elements sorption to iron oxyhydroxide: Model development and application to groundwater. *Appl. Geochem.* **87**, 158–166.

Lozano A., Fernández-Martínez A., Ayora A. and Poulain A. (2018) Local structure and ageing of basaluminite at different pH values and sulphate concentrations. *Chem. Geol*. **496**, 25-33.

Luo Y. R. and Byrne R. H. (2001) Yttrium and rare earth element complexation by chloride ions at 25 degrees. *C. J. Solution Chem.* **30** (9), 837–845.

Luo, Y.R., Byrne, R.H., (2004). Carbonate complexation of yttrium and the rare earth elements in natural rivers. *Geochim. Cosmochim. Acta* **68**, 691–699.

Luo, Y., Millero, F.J. (2004). Effects of temperature and ionic strength on the stabilities of the first and second fluoride complexes of yttrium and the rare earth elements. *Geochim. Cosmochim. Acta* **68** (21), 4301–4308.

Marmier N., Dumonceau A. J. and Fromage F. (1997) Surface complexation modeling of Yb(III) sorption and desorption on hematite and alumina. *J. Contam. Hydrol.* **26**, 159–167.

Marmier N. and Fromage F. (1999) Comparing electrostatic and non-electrostatic surface complexation modeling of the sorption of lanthanum on hematite. *J. Colloid. Interface Sci.* **212**, 252–263.

Masuda A., Kawakami O., Dohmoto Y.,Takenaka T. (1987) Lanthanide tetrad effects in nature: two mutually opposite types, W and M. *Geochem. J*. **21**, 119–124

Millero, F. J. (1992) Stability constants for the formation of rare earth inorganic complexes as a function of ionic strength. *Geochim. Cosmochim. Acta* **56**, 3123–3132.

Morgan, B., Johnston, S. G., Burton, E. D., Hagan, R. E. (2016) Acidic drainage drives anomalous rare earth element signatures in intertidal mangrove sediments. *Sci. Total Environ.* **573**, 831-840.

Noack C. W., Dzombak D. A., Karamalidis A. K. (2014) Rare earth element distributions and trends in natural waters with a focus on groundwater. *Environ. Sci. Technol*. **48**, 4317–4326.

Ohta A. and Kawabe I. (2000a) Rare earth element partitioning between Fe oxyhydroxide precipitates and aqueous NaCl solutions doped with $NaHCO_3$: Determinations of rare earth element complexation constants with carbonate ions. *Geochem. J.* **34**, 439-454.

Ohta A. and Kawabe I. (2000b) Theoretical study of tetrad effects observed in REE distribution coefficients between marine Fe– Mn deposit and deep seawater, and in REE(III)-carbonate complexation constants. *Geochem. J.* **34**, 455–473.

Pagano G., Guida M., Tommasi F., Orce R. (2015) Health effects and toxicity mechanisms of rare earth elements. Knowledge gaps and research prospects. *Ecotoxicol. Environ. Saf*. **115**, 40-48.

Pourret, O.; Martinez, R. E. (2009) Modeling lanthanide series binding sites on humic acid. *J. Colloid Interface Sci.* **330** (1), 45–50.

Pourret, O.; Davranche, M. (2013) Rare earth element sorption onto hydrous manganese oxide: A modeling study. *J. Colloid Interface Sci.* **395** (1), 18–23.

Parkhurst D. L. and Appelo C. A. J. (1999) User´s guide to PhreeqC (version 2.18) A computer program for speciation, and inverse geochemical calculations, U.*S. Department of the Interior, U.S. Geological Survey.*

Quinn K. A., Byrne R. H. and Schijf J. (2006a) Sorption of yttrium and rare earth elements by amorphous ferric hydroxide: influence of pH and ionic strength. *Mar. Chem.* **99**, 128–150.

Quinn K. A., Byrne R. H. and Schijf J. (2006b) Sorption of yttrium and rare earth elements by amorphous ferric hydroxide: influence of solution complexation with carbonate. *Geochim. Cosmochim. Acta* **70**, 4151–4165.

Rabung T., Geckeis G., Jim J and Beck H.P. (1998) Sorption of Eu(III) on natural hematite: application of surface complexation model. *J. Colloid Interface Sci*. **208**, 153-161.

Rabung, Th. Stumpf, H. Geckeis, R. Klenze and J. I. Kim (2000) Sorption of Am(III) and Eu(III) onto γ-alumina: experiment and modeling. *Radiochim. Acta* **88**, 711–716.

Rabung, B. T.; Geckeis, H.; Wang, X. K.; Rothe, J.; Denecke, M. A.; Klenze, R.; Fanghänel, T. (2006) Cm (III) sorption onto γ -Al_2O_3: New insight into sorption mechanisms by time-resolved laser fluorescence spectroscopy and extended X-Ray absorption fine structure. *Radiochim. Acta* **94**, 609–618.

Rouse, R. C.; Peacor, D. R.; Essene, E. J.; Coskren, T. D.; Lauf, R. J. (2001) The new minerals levinsonite-(Y) [$(Y,Nd,Ce)Al(SO_4)_2(C_2O_4)\cdot 12H_2O$] and Zugshunstite-(Ce) [(Ce,Nd,La)$Al(SO_4)_2(C_2O_4)\cdot$2H2O]: coexisting oxalates with different structures and differentiation of LREE and HREE. *Geochim. Cosmochim. Acta* **65**, 1101–1115.

Rudolph W. W. and Pye C. C. (2000) Raman spectroscopic measurements of scandium(III) hydration in aqueous perchlorate solution and ab initio molecular orbital studies of scandium(III) water clusters: Does Sc(III) occur as a hexaaqua complex? *J. Phys. Chem.* **104**, 1627-1639.

Schijf J. and Byrne R. H. (2004) Determination of SO4β1 for yttrium and the rare earth elements at I = 0.66 m and t = 25°C—Implications for YREE solution speciation in sulfate-rich waters. *Geochim. Cosmochim. Acta* **68** (13), 2825-2837.

Spahiu K., Bruno J. (1995) A selected thermodynamic database for REE to be used in HLNW performance assessment exercises. *SKB Technical Report*, 95-35, 88 pp.

Swallow, K.C., Hume, D.N., Morel, F.M.M. (1980) Sorption of copper and lead by hydrous ferric oxide. *Environ. Sci. Technol*. **14** (11), 1326–1331.

Tang, J.; Johannesson, K. H. (2003) Speciation of rare earth elements in natural terrestrial waters: Assessing the role of dissolved organic matter from the modeling approach. *Geochim. Cosmochim. Acta* **67** (13), 2321–2339.

Tochiyama O., Yamazaki H., Li N. (1996) Effect of the concentration of metal ions on their adsorption on various hydrous iron and aluminum oxides. *J. Nucl. Sci. Technol*. **33** (11): 846–851.

USGS (2018) U.S. Mineral Commodity Summaries 2018. *U.S. Geological Survey*, 196 pp.

Verplanck P. L., Antweiler R. C., Nordstrom D. K., Taylor H. E. (2001) Standard reference water samples for rare earth element determinations. *Appl. Geochem.* **16**, 231–244.

Verplanck P. L., Nordstrom D. K., Taylor H. E. and Kimball B. A. (2004) Rare earth element partitioning between hydrous ferric oxides and acid mine water during iron oxidation. *Appl. Geochem*. **19**, 1339– 1354.

Viadero Jr., R.C., Wei, X., Buzby, K.M. (2006) Characterization and dewatering evaluation of acid mine drainage sludge from ammonia neutralization. *Environ. Eng. Sci*. **23** (4), 734–743.

Webster, J. G., Swedlund, P. J., Webster, K. S. (1998) Trace metal adsorption onto an acid mine drainage iron(III) oxy hydroxy sulfate. *Environ. Sci. Technol.* **32***,* 1361–1368.

Williams T. and Kelley C. (1986) An interactive Plotting Program.

Wood S. A. and Samson A. M. (2006) The aqueous geochemistry of gallium, germanium, indium and scandium. *Ore Geol. Rev.* **28**, 57-102.

Xiangke W., Dong W., Xiongxin D., Wang A., Du J. and Tao Z. (2000) Sorption and desorption of Eu and Yb on alumina: mechanisms and effect of fulvic acid. *Appl. Radiat. Isot*. **52**, 165-173.

FIGURE CAPTIONS

Fig. 1. Sorption edges of (A) sorption with 20 mM of sulfate, (B) sorption with 0.5 mM of sulfate in solution. (Sc: squares, Y: triangles, Lu: circles and La: diamonds). Uncertainties in pH measurements and in the sorbed fraction are considered as ±0.02 and from ±0.01 to ±0.08, respectively, indicated by error bars.

Fig. 2. Comparison of REE sorbed fraction dependence on sulfate concentration for four selected elements. Sorption with 0.5 mM SO_4 in red squares and sorption with 20 mM SO_4 in blue diamonds.

Fig. 3. Patterns of log K_D values showing lanthanide M-type tetrad effect. (A) solution with 20 mM SO_4; B) solution with 0.5 mM SO_4. (log K_D^{Sc*} = log K_D^{Sc} -2)

Fig. 4. Aqueous species distribution of Y and Sc with pH for a solution with 20 mM (A,C) and 0.5 mM (B,D) of sulfate at 25°C and atmospheric pCO_2.

Fig. 5. Regressions obtained from the experimental data plotted as Eq. 5. Measured pH values and activities calculated from the final concentrations. XOH are free available surface sites.

Fig. 6. Regressions obtained from experimental data from Sc element plotted according the linearized equations of reactions 6 for $ScSO_4^+$ (A) and for $Sc(OH)_2^+$ (B).

Fig. 7. Comparison between experimental data (symbols) and calculated fraction (lines) of the sorption edge curves for Sc, Y, La and Lu of the experiments with 20 mM SO_4 (diamonds) and with 0.5 mM SO_4 (squares). Continuous lines: total sorption, dashed lines: sorption of MSO_4^+ species and pointed lines: sorption of MCO_3^+. Calculations at 25°C and pCO_2 of 3.5, including the carbonate complexation constants listed in Table SI-6.

Fig. 8. Comparison between experimental data (symbols) and calculated fraction (lines of the sorption edge curves for Sc, Y, La and Lu at two different solid:liquid ratios (1 g/L the blue symbols and 0.25 g/L the green ones) and 20 mM SO_4. Calculations at 25°C and pCO_2 of 3.5, including the carbonate complexation constants listed in Table SI-6.

Figure

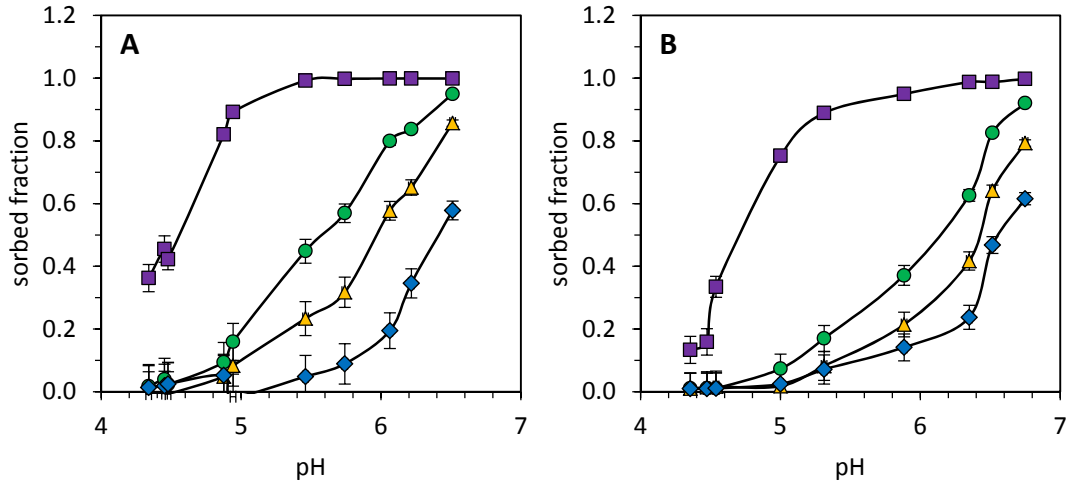

Figure 2

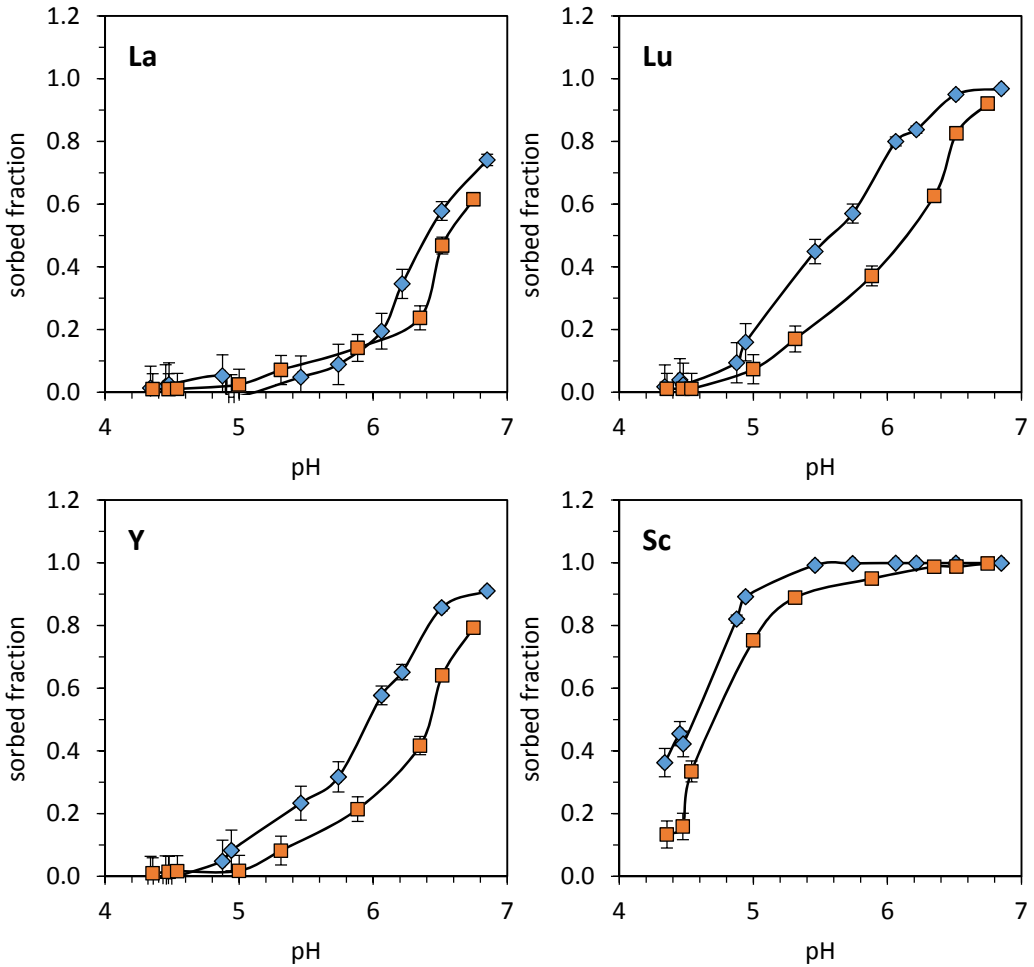

Figure 3

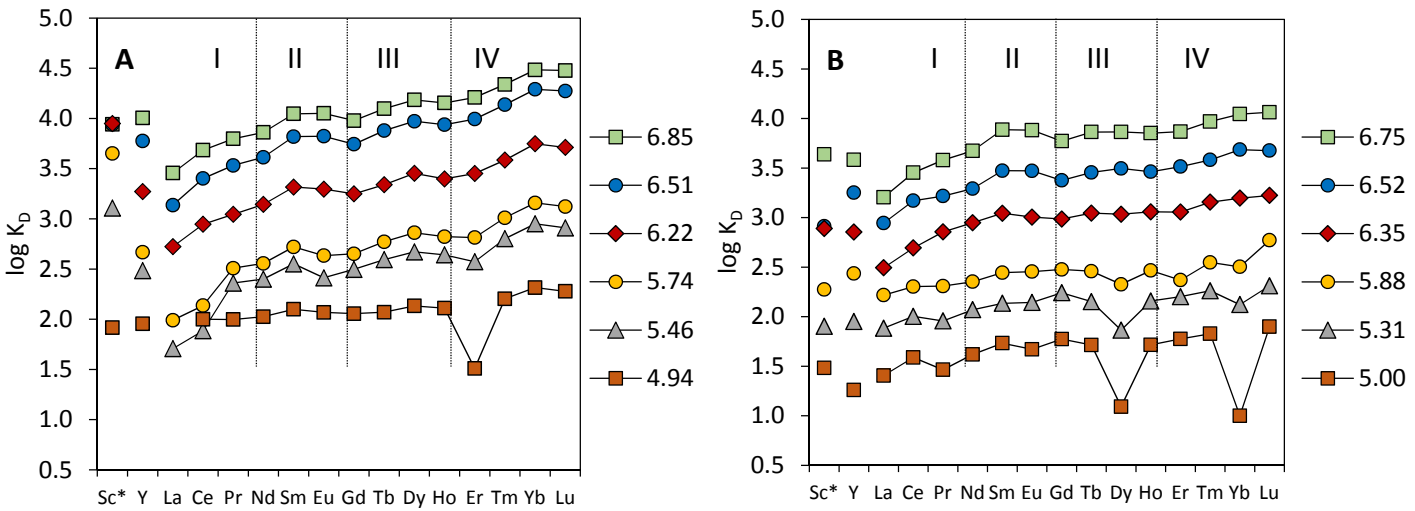

Figure 4

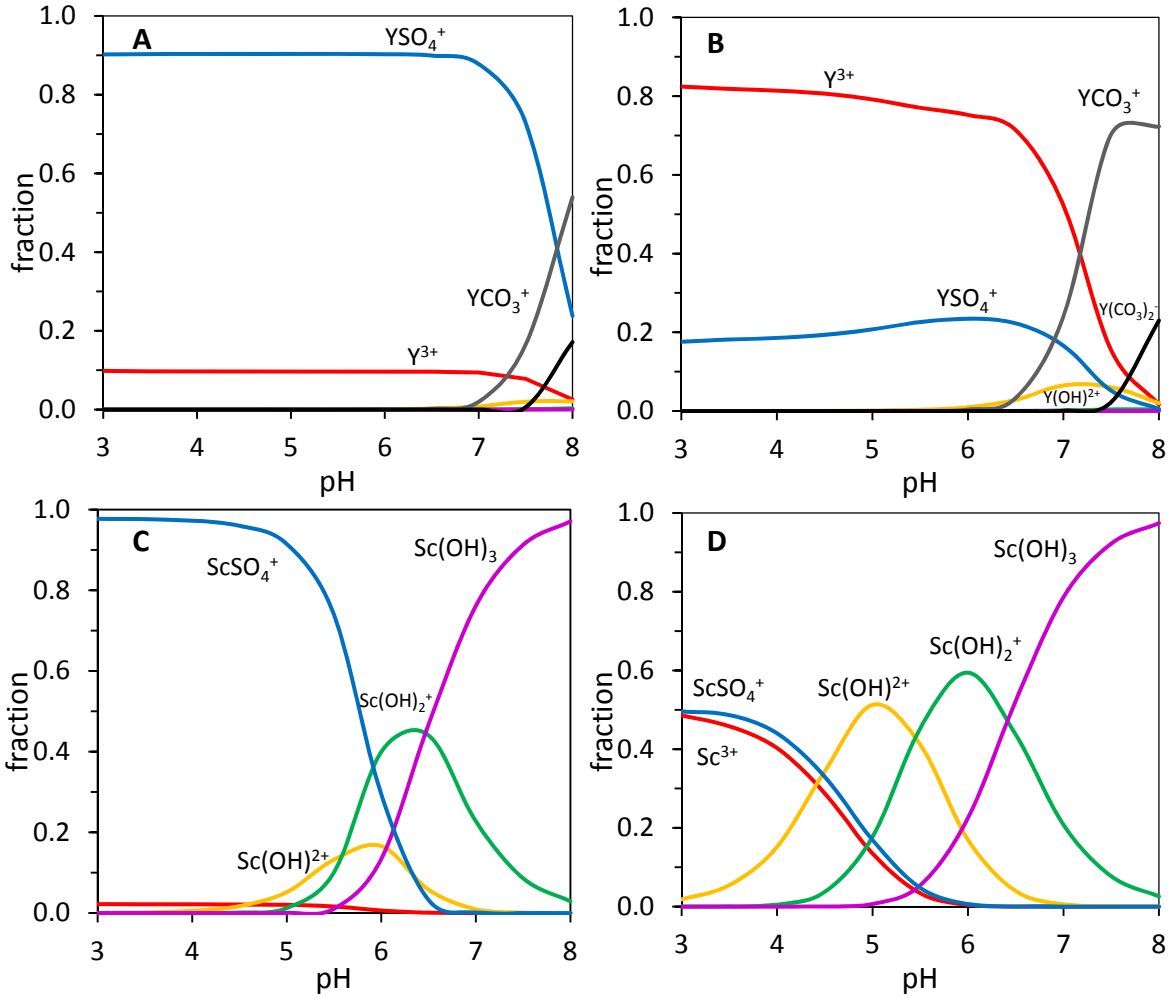

Figure 5

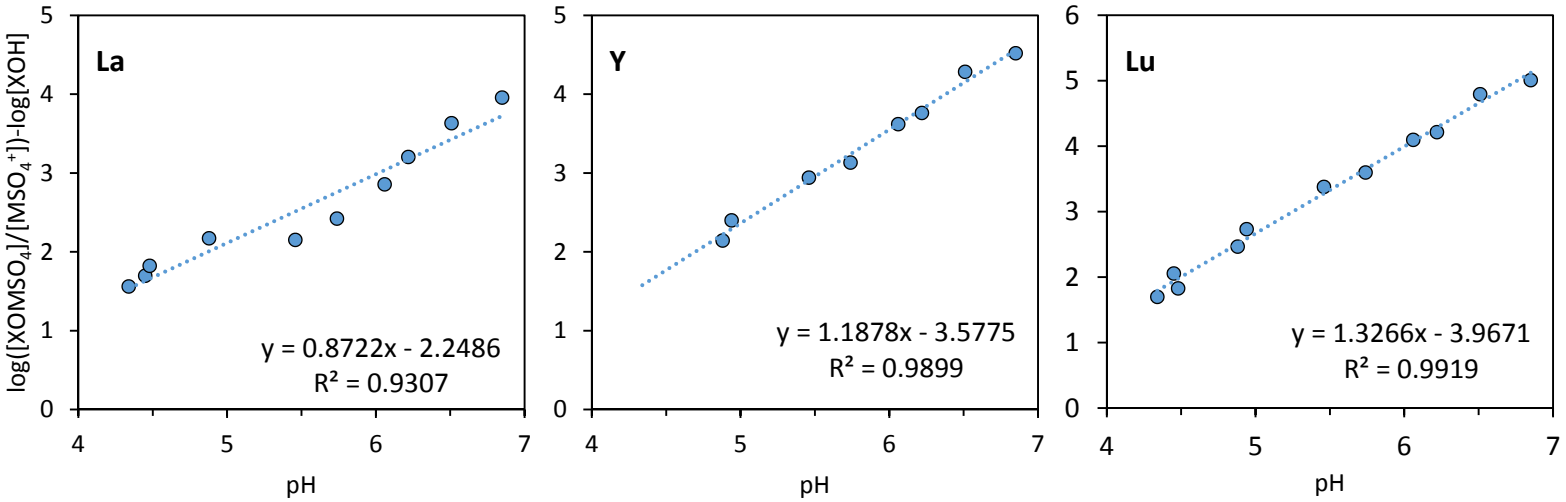

Figure 6

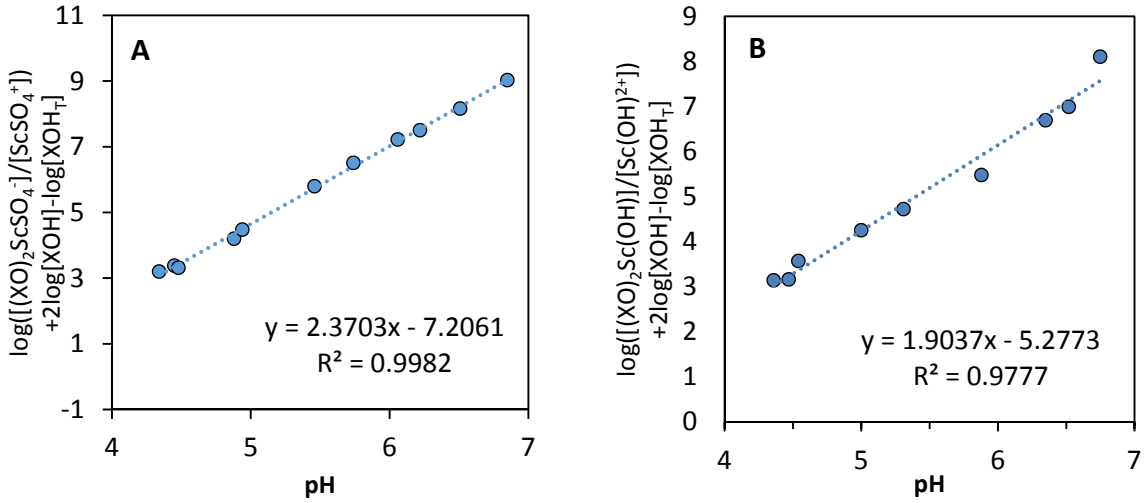

Figure 7

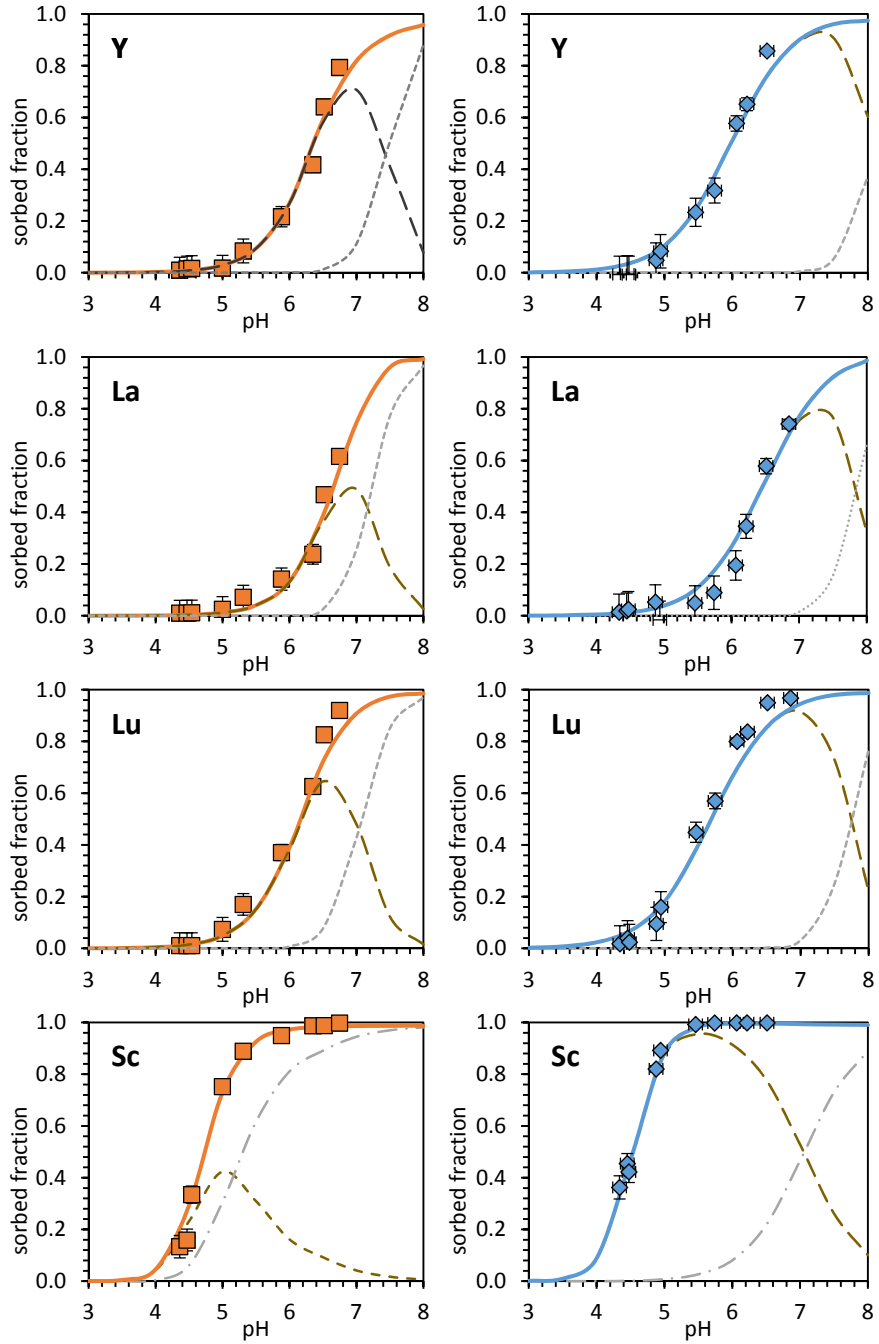

Figure 8

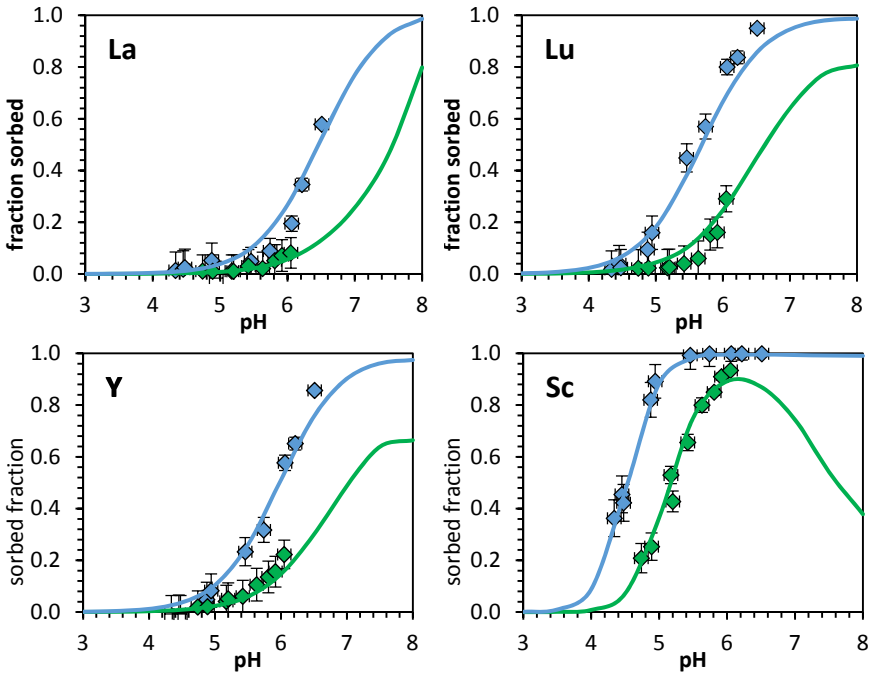

TABLE CAPTION

Table 1. Equilibrium constants for the formation of surface complexes (K_M of Eq. (3)) obtained by fitting the experimental values. Concentration of the surface species calculated as their molar fractions (i.e., K_M is the K_3 value of Wang and Giammar (2013)). Surface site density was 4.60 nm^{-2} and specific surface area 68 m^2/g.

Element	Surface Complex	Log $K_{M(SO4)}$	Error
Sc	$(XO)_2ScSO_4^-$	-5.19	0.08
	$(XO)_2Sc(OH)$	-5.81	0.09
Y	$XOYSO_4$	-2.48	0.06
La	$XOLaSO_4$	-2.95	0.08
Ce	$XOCeSO_4$	-2.81	0.07
Pr	$XOPrSO_4$	-2.69	0.05
Nd	$XONdSO_4$	-2.60	0.03
Sm	$XOSmSO_4$	-2.48	0.05
Eu	$XOEuSO_4$	-2.50	0.05
Gd	$XOGdSO_4$	-2.50	0.04
Tb	$XOTbSO_4$	-2.48	0.06
Dy	$XODySO_4$	-2.37	0.06
Ho	$XOHoSO_4$	-2.40	0.05
Er	$XOErSO_4$	-2.40	0.11
Tm	$XOTmSO_4$	-2.27	0.08
Yb	$XOYbSO_4$	-2.13	0.08
Lu	$XOLuSO_4$	-2.19	0.09